A new concept of inoculation by isomorphic refractory powders and its mechanism for grain refinement

Jacob Kennedy, Ahmed Kaci Boukellal, Etienne Brodu, Dominique Daloz, Bernard Rouat, Emmanuel Bouzy, Julien Zollinger

MTLA 36 (2024) 102167

Contents lists available at ScienceDirect

Materialia

journal homepage: www.elsevier.com/locate/mtla

Full length article

A new concept of inoculation by isomorphic refractory powders and its mechanism for grain refinement

J.R. Kennedy [a,b,c,*], A.K. Boukellal [a], E. Brodu [b,c], D. Daloz [a,b], B. Rouat [a,b], E. Bouzy [b,c], J. Zollinger [a,b]

[a] Université de Lorraine, Institut Jean Lamour, Department of Metallurgy & Materials Science and Engineering, Allée André Guinier - ARTEM Campus, F-54000 Nancy, France
[b] Laboratory of Excellence on Design of Alloy Metals for low-mAss Structures (DAMAS), Université de Lorraine, 57073 Metz, France
[c] Université de Lorraine, CNRS, Arts et Métiers ParisTech, LEM3, F-5700 Metz, France

ARTICLE INFO

Keywords:
Inoculation
Grain refinement
TiAl alloys
TKD
Casting
Solidification

ABSTRACT

Isomorphic Inoculation (ISI) is a novel grain refinement technique during solidification by the addition of metallic powders to the melt rather than ceramics. The powders are designed to grow epitaxially rather than to nucleate new solid, increasing theoretically the ratio between solidified grains and inoculants to 1:1. This technique circumvents the energy barrier problems related to heterogenous nucleation in traditional grain refinement techniques. In this manuscript, we show through a combination of numerical and experimental techniques that this ratio could be reached. This is achieved through novel experimental techniques to replicate the effects of the melt on the powders. A new CaF molten salt experiment was used to, for the first time, show the recrystallization/grain growth of Ti powders at high temperature. In parallel, we calibrated a model on our experimental conditions and used it to calculate the dissolution rate of the powders in the melt. The combined effects of grain growth, preferential grain boundary dissolution (increasing the number of powders) and bulk dissolution (decreasing the number of powders) act together, bringing the number of particles present during solidification near that of the number of solidified grains found in the sample ingots. The per particle efficiency of this method is far in excess of traditional inoculation methods and has the potential for wide applications, especially in systems such as TiAl used here where the heterogeneous particles remaining in the as-cast material are undesirable.

1. Introduction

The transformation of a polycrystalline material from liquid to solid is a complex process which can depend on a multitude of variables [1]. Since there is an energy barrier to nucleation it does not occur exactly at the melting temperature of the alloy but beneath it by a sufficient amount to account for this energy. Nucleation is of critical importance to the process of solidification and thus the structure of a material [2]. The energy barrier of formation for a nucleus can be significantly reduced by the presence of impurities or surfaces in the melt. The purposeful addition of such inhomogenaities into a metallic melt for the purpose of reducing the as cast grain size is known as inoculation [3]. Calculations using the spherical cap theory of nucleation do not agree with experimental results when the interfacial energy between the solid and liquid are very small [4]. It was shown that in these cases the nuclei were more accurately described as a single monolayer made up of atoms which form the solid on the substrate [5]. Nucleation can also be described in the case of small substrates as a thin film completely enveloping the substrate [6]. The role of pre-solidification order in the liquid in nucleation has also been investigated [7]. In each of these cases the substrate successfully reduces the energy barrier to nucleation, however it still exists. This is evidenced by the process of athermal nucleation, where at a given undercooling only particles of certain minimum size which is energetically favorable are active, particles smaller than this do not act unless the undercooling is increased to make nucleation more favorable [8]. In the case of these traditional undercooling dependent inoculants, not all powders added to the melt are active during solidification, as such the number of grains formed as a result of their addition is less than the number of powders added [8].

A new method of inoculation was developed to bypass the nucleation step of solidification and grain refine the as-cast structure without any heterogeneous particles remaining in the solidified matrix [9].

* Corresponding author at: Université de Lorraine, Institut Jean Lamour, Department of Metallurgy & Materials Science and Engineering, Allée André Guinier - ARTEM Campus, F-54000 Nancy, France.
E-mail address: jacob.kennedy@univ-lorraine.fr (J.R. Kennedy).

https://doi.org/10.1016/j.mtla.2024.102167
Received 5 April 2024; Accepted 29 June 2024
Available online 3 July 2024

This method, called isomorphic inoculation (ISI), is based on a novel concept. It uses specially designed powders which are of the same phase as the matrix with similar lattice parameters to promote direct epitaxial growth rather than nucleation of new solid [9]. This mechanism, which suppresses the nucleation step, was demonstrated during wire-arc additive manufacturing of Ti-6Al-4V where no interface was observed between a surviving particle and the solidifying surrounding β phase [10]. Inoculant alloys were designed with refractory metal additions to increase their survivability in the melt, inoculants containing both Nb and Ta were successfully implemented to grain refine a Ti-Al alloy, grain size reductions by up to a factor of three were observed. The difference in the macro and microstructure of an as-cast ingot with and without isomorphic inoculants is shown in Fig. 1. The grain refinement was greater than that of the alloying additions on their own (such as by solutal growth restriction from Nb additions). Further analysis also showed that there was not a direct 1:1 correlation between the number of powders added to the melt and the resultant as-cast grain size [11]. The number of new grains formed in the ingot by the inoculation process was greater than the number of powders added. This was predicted to be the result of a complex process by which the particles added to the melt broke up along grain boundaries [12] while also dissolving partially or totally, depending on their size. Evidence of such particle breakup was observed in a Ti-Ta inoculant powder designed to survive the Ti-Al melt. When imaging with backscattered electrons (BSE) for atomic contrast in an SEM the image contrast was adjusted and what appeared to be a single homogeneous powder could be seen to be in the process of breaking into multiple smaller particles, a composite image of this is shown in Fig. 2.

To gain understanding of this phenomena the microstructure of the cryo-milled Ti-Al-Nb alloy powder particles used as inoculants were characterized using on-axis Transmission Kikuchi Diffraction (TKD). A method of heat treatment using molten salts was developed in order to replicate the thermal conditions experienced by the particles in the TiAl melt to replicate and characterize the microstructure present during solidification. The dissolution of the inoculant alloy in the melt was approximated using the method of Hsu and Lin [13] taking into account fluid flow and validated experimentally with a bulk sample. The characteristics of the heat treated microstructures and validated dissolution rates were then combined to predict the number of inoculant powder grains present during solidification. This was then compared to the number of solidified grains formed in experiments to confirm grain boundary dissolution and a fully active population of particles.

2. Materials and methods

2.1. Powder processing

The alloys presented in this work were prepared from pure metals (Al > 99.95%; Ti > 99.7%; Nb > 99.9%) by induction melting in a cold crucible, as described previously [9]. The inoculant alloy investigated was Ti-25Nb-10Al (at%) of which one ingot was prepared and processed into inoculant powders for all the trials. As all powders were produced from the same ingot and processed further, the as-cast microstructure does not act during the inoculation process and as such the initial TiAlNb ingot was not characterized. Drillings produced from the ingot were cryo-milled for periods ranging from 3 to 11 h to produce different size distributions of powders to be used in the inoculation trials. Each sample was characterized by SEM image analysis to evaluate their size distributions. Further details of the experimental inoculation methodology can be found in previous works [9,11].

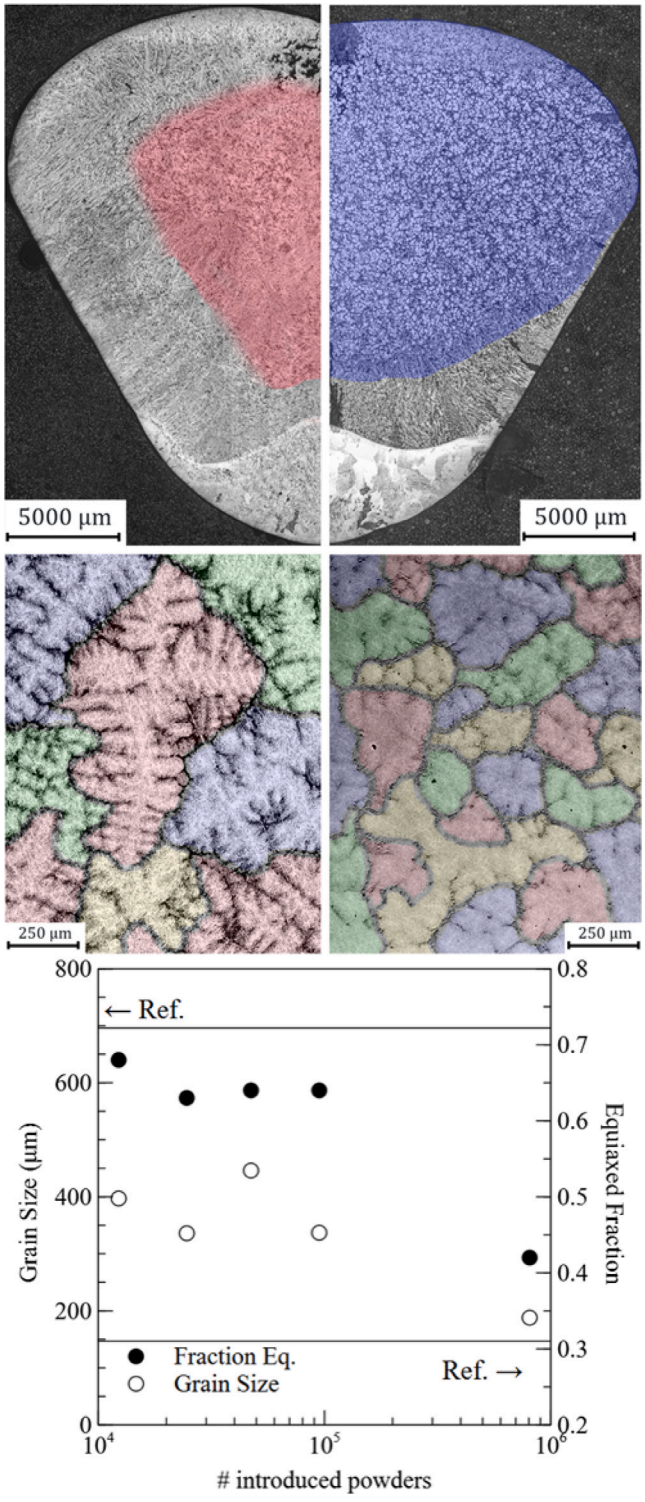

Fig. 1. Optical BF micrographs showing increase of equiaxed fraction from reference to sample inoculated with isomorphic inoculants (3 hr cryomilled Ti-Al-Nb) and corresponding SEM BSE images showing reference grain size and refined structure with the same inoculation alongside a plot showing the evolution of grain size and equiaxed fraction with increasing number of powders added.

2.2. Replicating thermal conditions of melt processing

An experimental set-up has been designed to simulate the thermal conditions of the inoculation process undergone by the Ti-Al-Nb powders in order to quantify their microstructure evolution. To do

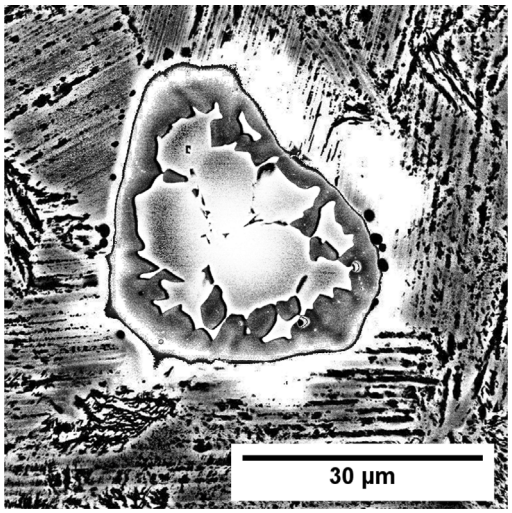

Fig. 2. Layered SEM BSE images with adjusted contrast of TiTa particle remaining in solidified ingot to show process of powder breakup.

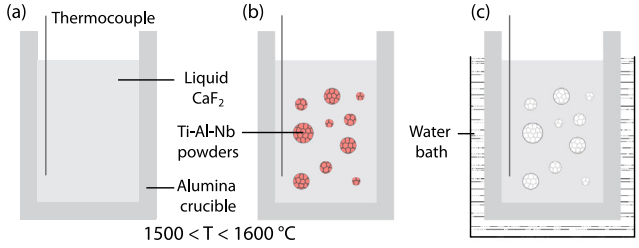

Fig. 3. Experimental schematic for heat treatment of particles, (a) molten salt at temperature, (b) addition of particles and (c) quenching.

so several challenges needed to be solved simultaneously, namely the experiment must: (i) reach high temperatures reflective of the melt, $1500 < T < 1600$ °C, (ii) survive at such temperatures for short to moderate heating times (iii) have fast heating rates reflective of the particles being introduced to the melt, and (iv) prevent oxidation of Ti-based alloy micron scale powders. The experiment that has been developed, although simple, meets these four criteria. The details of which are shown schematically in Fig. 3. High purity calcium fluoride (CaF_2 > 99.95%) was heated, and melted, at 100 K/min in an alumina crucible to 1500 and 1600 °C then held for 30 min to reach thermal equilibrium in an argon atmosphere (Fig. 3(a)). The powders were then introduced into the molten salt for different holding times ranging from 20 to 300 s before quenching the crucible into a water bath (Fig. 3(b) and (c)). A thermocouple was placed into the molten salt to measure the temperature evolution, upon cooling an average cooling rate of 150 K/s was measured. After cooling, a glass matrix is obtained containing the heat treated powders which can be sectioned and prepared metallographically for analysis. The powders used in this experiments were milled for 3 h and 9 h to investigate the influence of milling on the microstructure evolution. To ensure that the introduction of the powder into the molten salt does not affect the system temperature, the mass of Ti-Al-Nb powder introduced was small compared to the mass of CaF_2, typically 500 mg of powders for 10 g of CaF_2. Considering the typical size of the powders is roughly 100 µm, and a thermal diffusivity of $\alpha_T = 7.10^{-6}$ m^2 s^{-1} at 1600 °C [14] , a typical time to reach thermal equilibrium would be 1.43 ms, significantly smaller than the holding times, the heating stage can then be neglected in the following analyses.

2.3. Rod dipping

In order to analyze the interface between Ti-Al-Nb and Ti-Al after the two have interacted in similar conditions to the inoculation trials a rod of Ti-Al-Nb was manufactured and dipped into molten Ti-Al. The rod was formed by vacuum pulling an ingot of Ti-Al-Nb into a silica tube with an inside diameter of 5 mm. The same procedure was used as in the inoculation trials but with the Ti-Al-Nb rod in place of the inoculating pellet, the rod was positioned away from the bulk alloy until the alloy was fully molten then inserted directly into the melt and held at temperature for 20 s before the furnace power was turned off and the melt allowed to solidify. The solidified ingot with the intact rod in its core could then be sectioned and characterized to evaluate the alloy interaction and dissolution rate in the melt.

2.4. Characterization

The size of the powders used in each inoculation trial were characterized by image analysis from SEM images, details of which are provided in [9]. However, the structure of the as-cryo-milled inoculant powder is an ultra-fine structure, so much so that conventional EBSD does not have the spatial resolution sufficient to resolve its details. Transmission Kikuchi Diffraction (TKD) [15,16] is an appropriate method for analyzing such microstructures as it is possible to obtain a spatial resolution of a few nm, an order of magnitude better than that of EBSD. In addition, the diffraction patterns are of better quality because as the interaction volume is much smaller it contains fewer defects and elastic distortions. The TKD setup was of the on-axis configuration, which was designed and validated at the LEM3 in Metz, where the scintillator is located beneath the sample perpendicular to the electron beam, resulting in high intensity diffraction patterns [17]. In addition to the detector for the Kikuchi bands there are also three diodes for forward scattered electron detection (FSD). Each diode produces a single color. When an image is formed from all three detectors it is extremely sensitive to changes in orientation. TKD was performed using a Zeiss Supra 40 at 30keV, a working distance of 5-7 mm, and a sample to detector distance of 20 mm. Orientation maps were acquired using a step size of 4 nm. Analysis of the orientation data was conducted using the free software package ATEX developed at the LEM3 [18]. The microstructure of the particles were also evaluated after the molten salt heat treatment by SEM imaging with BSE. The dissolution of the Ti-Al-Nb rod was evaluated by optical microscopy.

3. Results

3.1. Grain size evolution with milling time

Representative TKD results from powders which were milled for 3 h and 9 h are shown in Fig. 4. The unindexed regions (black pixels) appear mostly along grain boundaries as 2 patterns corresponding to each grain are often overlapping in these regions making them more difficult to index. 100% of the patterns indexed for both 3 h and 9 h cryomilled powder particles correspond to the β phase. As the Ti-10Al-25Nb inoculant ingot was 100% β phase, that means that the cryo-milling did not induce a phase transformation.

As we can see in Fig. 4, the morphology of the microstructures of both powders have many common characteristics. The grains are greatly elongated in a direction roughly parallel the surface of the particles, which is perpendicular to the direction of impact during milling. This kind of morphology is a "pancake morphology" referring to the shape of the grains these "pancakes" are aligned along deformation bands. The grains are very fine, the thickness of the "pancakes" can be as little as 20 nm. There are differences between the two powder particles with regard to the size of the grains, their shape and the substructure within them. If a grain is defined as having a disorientation of more than 15° with its neighbors, the average grain size was found to

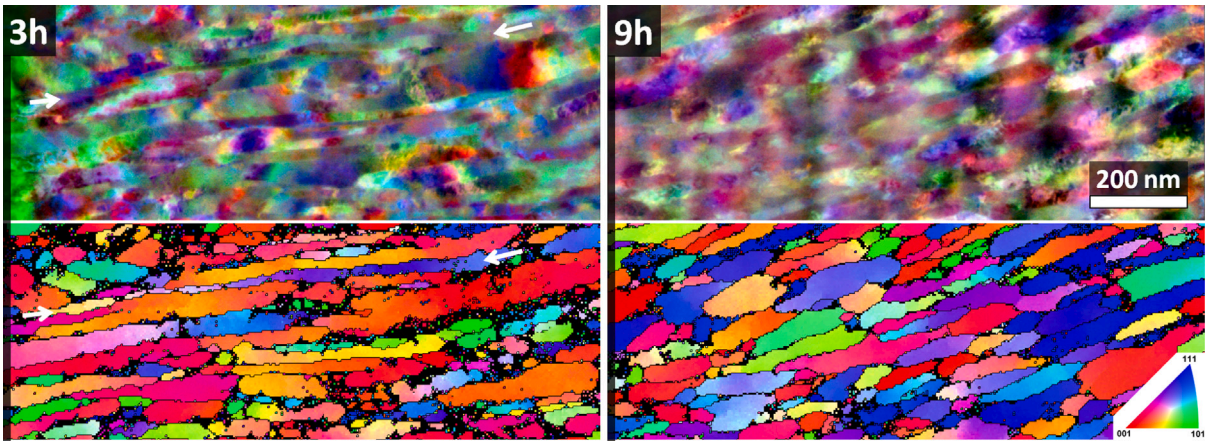

Fig. 4. Results of a characterization by on-axis TKD in SEM of two Ti-Al-Nb inoculants prepared by FIB, after 3 h (left) and 9 h (right) cryo-milling. The top line shows FSE images of the region investigated by TKD. The second line shows IPF orientation maps.

be 52 nm with a median size of only 38 nm for the 3 h milled sample and 43 nm and 34 nm for the 9 h milled sample. In the 9 h milled sample there are fewer long pancaked grains in either the FSD image or orientation map.

These microstructures are quite characteristic of strongly plastically deformed (SPD) materials such as those obtained by equal channel angular pressure (ECAP) or high pressure torsion (HPT) processes [19]. The evolution of microstructures during strong plastic deformation follows a very general pattern. First of all, at low strains, the grains get longer and form what are often referred to as bands of deformation. Then the different parts of a deformation band are subjected to heterogeneous deformations, i.e. different slip systems will operate in the different parts of the deformation band. As a result, geometrical necessary dislocations (GND) will form at the boundary between the two parts of the crystal to ensure the compatibility of the deformations [20], thus a substructure is formed inside the deformation bands. This is how the subdivision of the grains takes place [21]. As the deformation increases, the boundary disorientation increases due to the accumulation of dislocations and concomitantly the density of dislocations inside the grains decreases [22]. For the powders, we do not know the total strain accumulated in the repeated impacts during the milling but we know that it is relatively high because the grain subdivision process has already begun, it is in progress but has not yet reached its final stage. Even for the 9 h cryo-milled powder particles, the grains are still relatively elongated and the LAGB fraction is high (Fig. 5). This means that the long pancaked grains found after 3 h of milling are being subsectioned along their subgrain boundaries as milling continues. From this analysis it can be seen that the grain size of the particles does not change significantly as milling time increases. The internal grain structure changes, however when considering the microstructure of the particles in future analysis the initial grain size can be taken to be identical as the average grain sizes found in both were nearly identical and further milling only reduces the size slightly.

3.2. High temperature grain growth

The powders which were heat treated at 1600 °C had markedly different microstructure than the as milled powders. The pancaked structure seen by TKD was completely transformed into a mixed structure of large β grains in the centre of the powders with small α/γ lath colonies around the periphery. The prior β grain boundaries can be seen as the boundaries between the lamellar colonies, defined by similar directions of laths within a colony. While the microstructure of the powders change, during the heat treatment with molten salt the size of each powder will remain constant as there is no dissolution occurring i.e., there is little chemical reaction between the molten salt and powders. Representative micrographs from near the centre of two powders are shown in Fig. 6(a) for 3 h and (b) for 9 h milled particles. Additionally, not shown in the figure, the grain size appeared to be largest in the center of the powders, even if the center was lamellar, with smaller grains closer to the edge this is likely due to oxygen pickup during the heat treatment, which may have an effect on the grain growth occurring in the molten salt compared to the inoculation trials where grain growth occurs in the melt without oxygen pickup. These demarcations were identified manually and their areas measured using imageJ software. The size of the prior β grains was evaluated for the powder samples along with the size of the parent powder they were measured within, the results of which are shown in Fig. 6(c), the error reported being the standard deviation of the measurements. The powder size was taken to be the equivalent circular diameter of the powder cross sectional area evaluated. The average grain size found in the particles shown in Fig. 6 a and b was 46 and 38 μm respectively, both had powder diameters close to 400 μm.

For the 300s heat treatment 20 powders of 3hr milled Ti-Al-Nb and 17 powders of 9hr milled were found with cross sections that had discernible β grain structures. The average β grain size found was 82 μm across both samples, 76 μm for the 3 hr milled powder and 94 μm for the 9 hr. The average powder size was 282 μm for both milling times. The global average grain size was within error, taken as one standard deviation, for all the powders measured except the smallest 3hr powder. There does appear to be a slight trend of increasing β grain size as the powder size increases but it is not strong enough across the powders measured to be conclusive, especially since the spread of the grain sizes increases as well with powder size. The size of the powders seems to have a greater effect on the grain size than the milling time. Since all the powders have grain sizes which agree with the average the grain size can be taken to be the same between the 3hr and 9hr powders after extended high temperature exposure. This means that the change in the subgrain structure seen in the as-milled powders does not have a large effect on the grain size after this treatment, once again indicating that the main effect of extended milling times is a reduction of powder size and does not have a strong effect on the microstructural properties.

For the 20 s heat treatment fifteen powders from each milling time were measured, their size and grain size evaluated in the same manner as the longer duration heat treatment. The average grain size of the three hour milled samples was 44 μm while it was only 31 μm for the nine hour milled powders. The overlap in the size of the powders measured is smaller than in the extended time experiment, the three hour powders measured had an average size of 360 μm while the nine hour powders averaged 305 μm. The global average grain size of 37 μm does not appear to agree as well with all the particles as the global average did for the extended hold time, however all the sizes

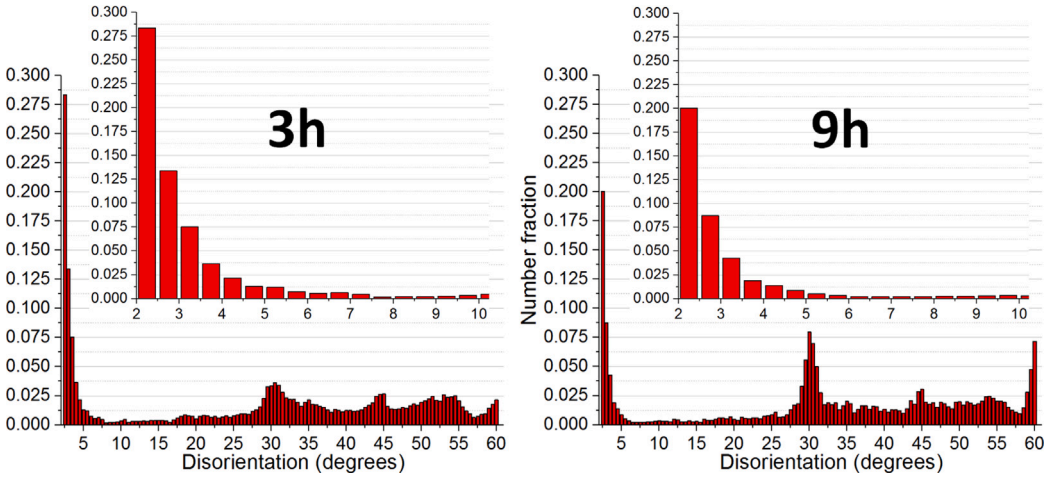

Fig. 5. Grain misorientation histograms obtained by TKD of (a) 3hr and (b) 9hr cryomilled Ti-Al-Nb particles.

agree well with a linear trend of increasing grain size with increasing powder size. This could be the result of a surface effect leading to the aforementioned smaller grain sizes along the surface of the powders compared to their centers. Again this indicates that the size of the powders has a larger effect on the grain size after thermal treatment than the differences in the initial microstructure.

It was determined that the grain size of the powders after thermal treatment did not change significantly as milling time of the powders increased. The size of the powders was seen to have a greater effect on the grain size than the milling time. The grain size/powder size relation found after 20 s of interaction time at 1600 °C can be used to more accurately predict the grain size within the powder size distributions and number of grains introduced in each of the inoculation trials.

The grain growth kinetics, neglecting the heating stage of the particles, can be modeled using the approach of Malow and Koch [23]:

$$d^n - d_o^n = k\ t = k_o\ t\ \exp\left(-\frac{Q}{RT}\right) \tag{1}$$

where d_o and d are the grain diameters before and after thermal treatment respectively, k a rate constant, Q the grain growth activation energy, t the time, n the growth exponent, R the ideal gas constant and T the temperature. In the present case, d_o can be neglected as it nears zero in comparison to d and parabolic growth is assumed ($n = 2$). Dividing both side of Eq. (1) by the square of the particle size gives a direct relation between a dimensionless grain size, Δ, and a Fourier number for grain growth, Fo:

$$\Delta^2 = \frac{d^2}{d_p^2} = \frac{k_o\ t\ \exp\left(-\frac{Q}{RT}\right)}{d_p^2} = Fo \tag{2}$$

The evolution of Δ with Fo is given in Fig. 6(d). From these data, the values of k_o and Q were determined as 10^{-4} m^2/s and 320 kJ, respectively. While there is currently no data available at such high temperature in the literature, there is a reasonable agreement with data for β-Ti alloyed with refractory elements [24].

3.3. Rod dipping experiment

Optical microscopy was performed on transverse and longitudinal cross sections of the TiAlNb rod after dipping. Dendritic growth from the rod can be seen optically from a transverse cross section near the top of the rod in Fig. 7a. The diameter of the rod after dissolution was measured along its length, the results of which are shown in Fig. 7b. The dissolution of the rod was most pronounced at its top and bottom. This is likely due to the 3D nature of the experiment, dissolution occurring from more directions at the bottom corners of the rod and the effect of fluid flow loops increasing dissolution at the top. The Diameter of the rod was found to have decreased on average by 180 μm which corresponds to a dissolution length of 90 μm.

4. Mechanism

4.1. Modeling dissolution

Prediction of powder dissolution in the melt requires a sophisticated mathematical model taking into account the induction induced stirring effects, namely the complex motion in a 3D fluid flow. Such a model is beyond the scope of this paper. Instead, we adapt Hsu and Lin's model [13] to evaluate how dissolution is affecting the ISI powders in the melt. The model assumes (1) a solid particle to be spherical, (2) a surface layer to be formed near the solid–liquid interface and, (3) the rate limiting solute for dissolution process is Nb diffusion as it is the slowest diffuser in the system Ti-Al-Nb. The Nb concentration C_l^* at the surface of a particle of radius r_c on the liquid side is assumed to be saturated and could thus be taken from the phase diagram [25], while the concentration in the bulk liquid C_l^0 is assumed to be 0, as the melt is Ti-Al. The distance between the regions corresponding to C_l^* and C_l^0 respectively is the mass transfer boundary layer, δ. In this case according to film theory [26], the solute transport equation is given by

$$\frac{\partial C}{\partial t} = \frac{D_L}{r}\frac{\partial}{\partial r}\left(r^2\frac{\partial C}{\partial r}\right) \tag{3}$$

where D_L is Nb diffusion coefficient in the liquid phase and r is the distance measured from the center of the particle. To account for the solute build up effects, we use the model developed by Hsu and Lin that considers the liquid volume interaction with the solid [13]. The derivation of this model leads to

$$\frac{dr^*}{dt^*} = -\frac{(r^* + \delta^*)(C^* - 1 + r^{*3})}{\delta^* r^*}. \tag{4}$$

In Eq. (4), $\delta^* = \delta/r_0$, $r^* = r_c/r_0$ and $C^* = (C_l^* - C_l^0)/((4\pi\rho_s r_0^3 N)/(3VM))$ where r_0 is the initial radius of the powder, N the number of powders, V the volume of liquid, ρ_s the powder density, and M the molar weight of the solute. The detailed solution for the model to calculate the dissolution rate assuming the initial condition $r^* = 1$ at $t^* = 0$ can be found in [13]. Such a solution relies on a fixed value of δ, that is a prior unknown in our problem. To calculate δ, we take into account the fluid flow, which makes δ dependent on the hydrodynamic boundary layer δ_h, i.e. the distance from the powder to where the fluid velocity $U = 0.99\ U_{max}$, U_{max} being the free flowing velocity. In a laminar flow [27],

$$\delta = \frac{\delta_h D_L}{\nu} \tag{5}$$

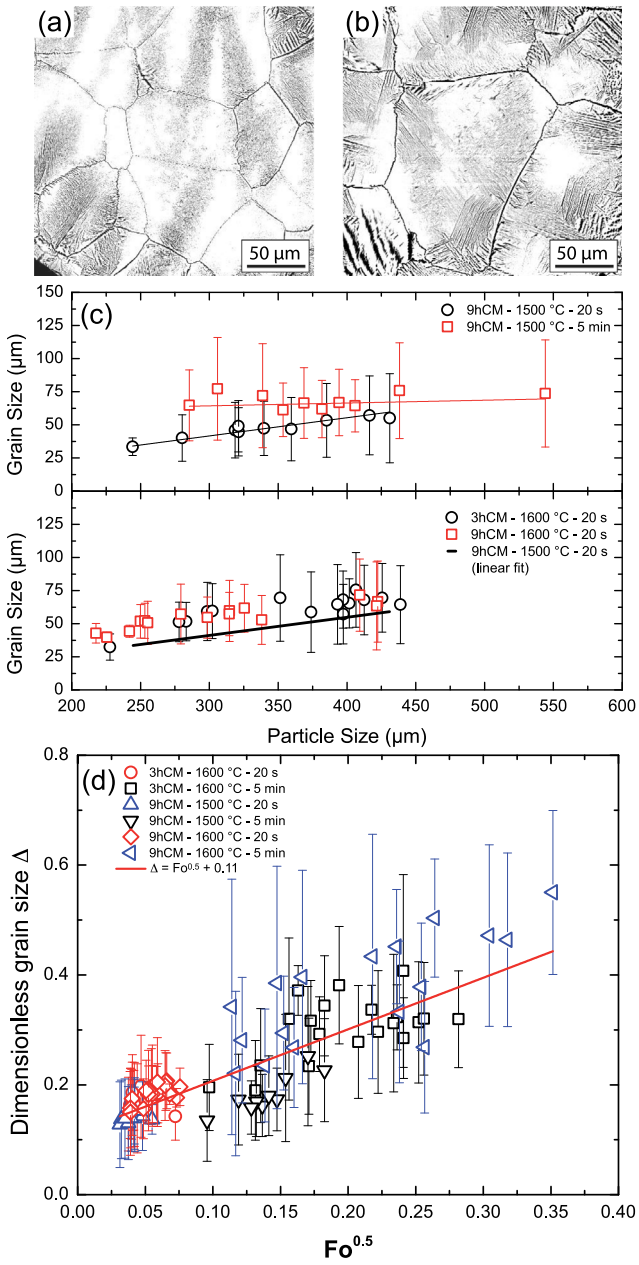

Fig. 6. SEM BSE micrographs of 400 µm diameter (a) 3 h and (b) 9 h cryomilled particles after 20 s at 1600 °C (c) Relationship between grain size and particle size with different thermal treatments and (d) Evolution of the dimensionless grain with the grain growth Fourier Number (see text for details).

where ν is the kinematic viscosity and $\delta_h = 5r_c/\sqrt{Re}$ with Re being the Reynolds number. The diffusion coefficient D_L is estimated using the Stokes–Einstein relation:

$$D_L = \frac{k_b T}{6\pi\eta r} \tag{6}$$

where k_b is the Boltzmann constant while

$$Re = \frac{2r_0 U_{max}}{\nu}. \tag{7}$$

The maximum relative velocity U_{max} occurs when gravity is acting against the fluid flow. In a moving reference frame it reads

$$U_{max} = \sqrt{\frac{8gr_0(\rho_s - \rho_L)}{3C_d\rho_L}} \tag{8}$$

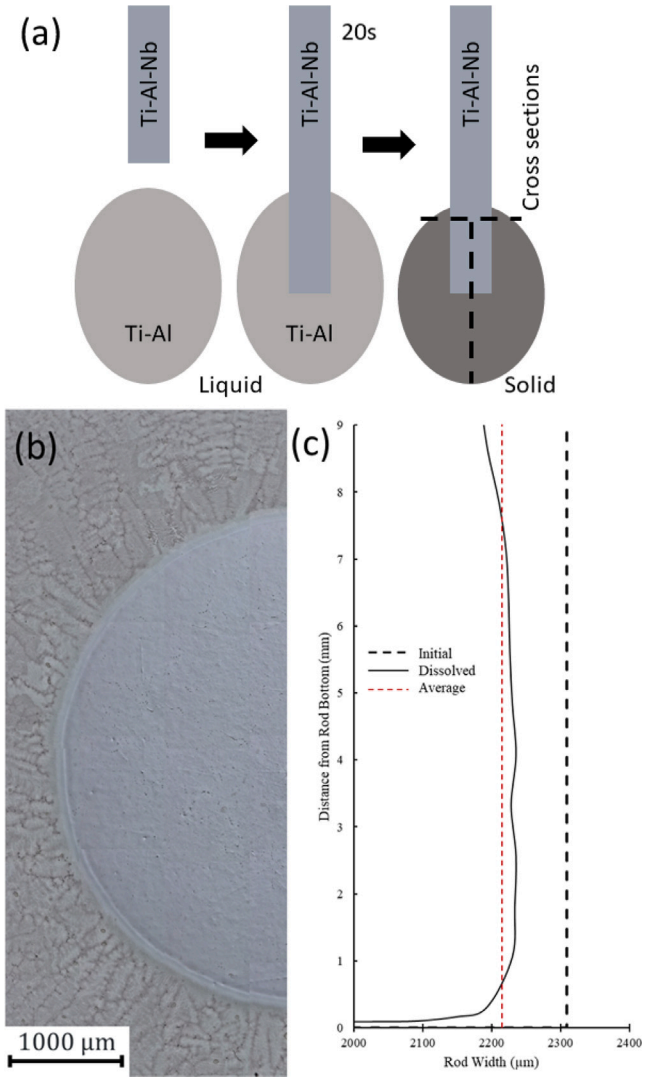

Fig. 7. (a) schematic of rod dipping, Rod/Bulk interface (b) optical bright field micrograph showing columnar growth from rod into the bulk, (c) Radius of the rod before and after dissolution.

where g is the acceleration due to gravity, ρ_s and ρ_L the powder and liquid density respectively and C_D the drag coefficient. The drag coefficient and Reynolds number rely on one another according to [28]:

$$C_d = \frac{24}{Re} \; if \; Re < 53 \tag{9}$$

$$C_d = 0.45 \; if \; Re > 53 \tag{10}$$

This relation makes finding the velocity an iterative process. The initial velocity to find a starting Reynolds number was taken to be the fluid velocity, i.e. assuming stationary powders. The calculations were iterated to find the velocity, Reynolds number and drag coefficient. Once relative velocities of the powders were found the size of the layer could be determined. The requisite data to apply the model to the rod dissolution are shown in Table 1, while the rod dissolution with time is plotted on Fig. 8(a) with solid lines. JK{While the rod has a different morphology than the particles, it was chosen as it is easily located in the ingot after solidification, allowing measurement of the dissolution length as compared to the addition of spherical particles which could not be so easily located to be measured. The calculation method was then validated using the experimental rod

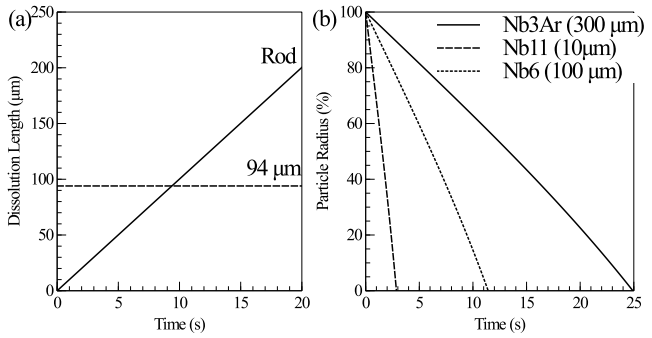

Fig. 8. Time evolution of (a) the dissolution length of a rod (solid line) and (b) the dissolution length of different sized particles milled for 3 (Nb3Ar) 6 (Nb6) or 11 (Nb11) hours with different initial radii (10, 100 and 300 μm). The dashed horizontal line in (a) corresponds the experimental dissolution length. Data corresponding to the calculations are gathered in Table 1.

Table 1
Data for rod dissolution calculations.

Variable	Symbol	Units	Value	Ref
Boundary Layer	δ_m	m	3.35×10^{-5}	calc.
Particle Radius	r_p	m	2.50×10^{-3}	PW
Number of Particles	N	–	1	PW
Nb Liquid Diffusion	D_L	m^2/s	2.14×10^{-9}	calc.
Liquid Volume	V	m^3	9.84×10^{-6}	PW
Particle Density	ρ_s	g/m^3	5.01×10^{6}	calc.
Liquid Density	ρ_L	g/m^3	3.82×10^{6}	[29]
Nb Molar Weight	M	g/mol	93	[30]
Nb Liquid Conc.	X^l_{Nb}	mol/m^3	0	PW
Nb interface Conc.	X^{le}_{Nb}	mol/m^3	8164	[25]
Kinematic Viscosity	ν	m^2/s	4.93×10^{-7}	[31]
Dynamic Viscosity	η	Pa s	1.88×10^{-3}	[31]
Temperature	T	°C	1600	PW

dipping experiment where the dissolution of the rod was measured after a known time at temperature. The rod spent roughly 10 s interacting with the melt at temperature during the 20 s experimental time. During those 10 s, the dissolution length was estimated to be 94 μm (dashed line on Fig. 8(a)). Assuming the liquid interaction volume was equal to that of the whole molten bulk alloy used in the experiment at 1600 °C (determined by comparing EDX compositions across the solid/liquid interface to ternary phase diagrams at different temperatures obtained with thermocalc), the calculated dissolution length after 10 s was 75 μm, slightly less than experimental dissolution length (94 μm). In order to get a dissolution length of 94 μm the model required an interaction time of 13 s. Considering the assumptions and uncertainties of the calculation and experimental dissolution time this is relatively good agreement between the calculation and measured values for the rod dipping experiment. The model can then be used to calculate the dissolution of the powders used in the inoculation trials. Indeed, on Fig. 8(b) examples of particle radii evolution (equivalent to dissolution length) with time are presented for three different initial particle classes (different initial radii r_0). According to this figure, particles with $r_0 >$ 100 μm do not dissolve completely within 10 s, while the ones with $r_0 <$ 100 μm do much earlier. However, the ones with $r_0 \backsim$ 100 μm do dissolve after roughly 10 s, in a good agreement with the experimental results.

4.2. Effect of dissolution and breakup on particle populations

The dissolution model and grain growth experiments can be used together to estimate the effect of dissolution and powder breakup on the population of isomorphic inoculants present during solidification in each inoculation experiment. The calculation uses the introduced powder size to find both the particle (grain) size within the powders and the dissolution length, effectively separating the dissolution and breakup phenomena into two independent processes in contrast to the real behavior of both occurring concurrently. However, modeling such concurrent processes would be significantly more complex and outside the scope of this paper. The microstructure and size of the introduced powders, assuming preferential grain boundary dissolution and full breakup of the powders along grain boundaries, is used to approximate the number of particles and their size present in the melt, while dissolution calculations are performed on these particles to determine if they survive until solidification to act as ISI.

The number of particles added to the melt in each trial is calculated from their size distribution, along with the mass added, assuming spherical powders. Each powder population was divided into ten size ranges and the average of each range was used for calculation. The dissolution model was applied to all these ranges to obtain a dissolution length for each. If the dissolution length is greater than the average radius of the powder in a range all powders in the range are considered to have dissolved. If the dissolution length is less than the average radius of the powder in a range it is subtracted from the radius and the reduced radius and number of powders used to calculate the volume of the remaining powder.

The size of each powder will be decreased not only by this radial dissolution but also particle breakup (as shown in Fig. 2). This may occur by preferential grain boundary dissolution [12] if the grain boundary energy is higher than that of two solid liquid interface i.e. $\sigma_{\beta}/\beta > 2(\sigma_{\beta}/\ell)$, which should be the case here as the Ti-Al-Nb grain boundaries after grain growth have a high misorientation angle and thus a high energy. The liquid will then fully wet along the grain boundary permitting separation of the particles in the melt along grain boundaries. For clarity henceforth the initial cryomilled particles will be referred to as powder and their internal grains as particles.

The grain growth behavior observed during the molten salt experiments was used to calculate the particle (grain) size within the powders after 20 s at 1600 ° C which could then be used to calculate the number of particles assuming 100% breakup along these grain boundaries. The number of particles after breakup is based on the assumption that powder breakup occurs independently of, and after, radial powder dissolution. The initial powder size is used to calculate the particle (grain) size within the powder rather than their size after dissolution. The number of particles is calculated by dividing the volume of powder in a given size range after dissolution by the volume of a grown grain (particle) assuming spherical powders and particles. This was then taken to be the number of particles remaining which could act during solidification. The calculated grain sizes can be considered reasonable as they correlate well with sizes found during the experiments, i.e., the smallest calculated grain size, > 3 μm within 22 μm powders, is not significantly smaller than the smallest grain found experimentally, 4 μm within a powder > 100 μm

4.3. Isomorphic inoculation mechanism from cryo-milled powders

Assuming all particles/powders present during solidification are active and each is responsible for the formation of a single grain (1 1 ratio), knowing the equiaxed fraction of each ingot (volume) and assuming spherical grains an as-cast grain size can be predicted given different assumptions, as shown in Figure 9a. There is then a correlation between the predicted grain size and the number of grains forming, a larger predicted grain size means fewer grains forming than a smaller. If the predicted grain size is larger than the experimental, assuming a 1 1 ratio, there are fewer active ISI predicted than present. This can help make more clear the effects of the assumptions used. If the powders are unaffected by the melt, the number of grains formed would be equal to the number of powders added to the melt, however, this assumption predicts a much larger grain size than found experimentally, larger even than the grain size found experimentally without ISI addition. Thus this predicts too few active ISI. It is then evident that the powders

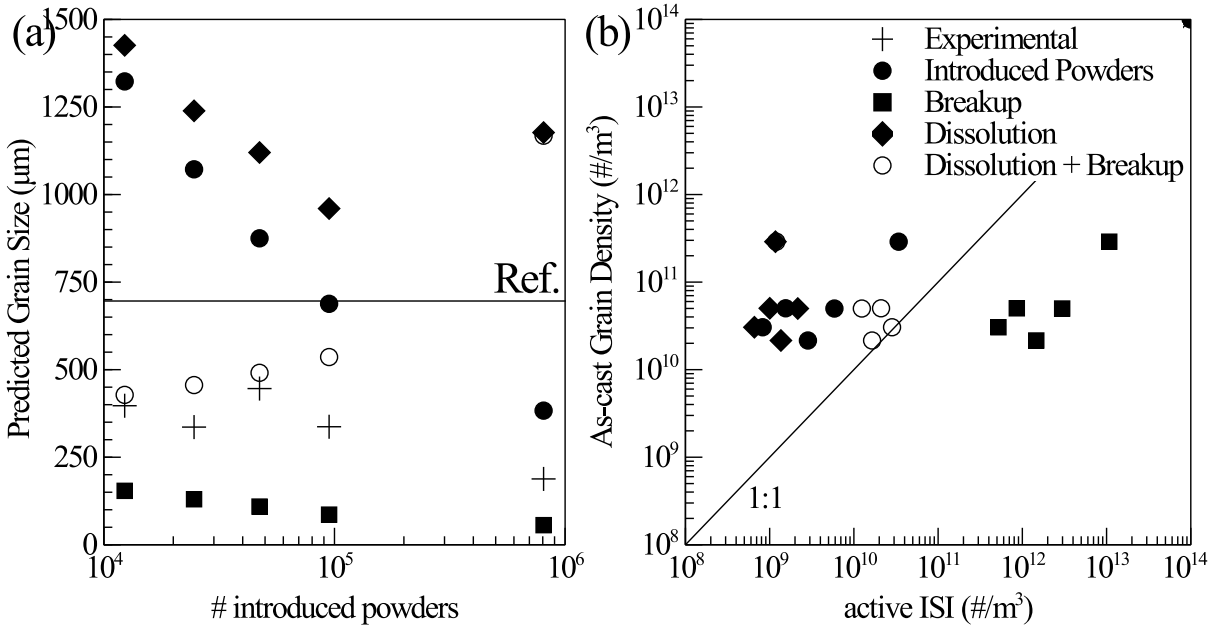

Fig. 9. (a) Relationship between introduced particles and predicted grain size and (b) Particle grain density and equiaxed grain density considering experimental results and calculations with different active phenomena.

are affected by the melt. If it is assumed that interaction with the melt results in only grain growth and breakup (Breakup) the predicted grain size is much smaller than experimental, a overestimation of the number of active ISI. If only dissolution is considered (Dissolution) then the predicted grain size is even larger than if no interactions are considered. If both these phenomena are considered (Dissolution + Breakup) the predicted grain size is relatively close to the experimental, except for the case of the largest number of introduced powders. This corresponds to the 11 h milled sample which has the smallest size distribution. This over estimation of the grain size is due to the large fraction of powders which were calculated to dissolve, less than 2% (by number) of the particles introduced were calculated to survive until solidification. This is likely an overestimation of the dissolution as only the initial particle conditions are considered in the dissolution calculations. A more robust model would consider the change in velocity and boundary layer as dissolution occurs which would likely decrease the complete dissolution of small particles.

If the particles are acting as centers of direct particle growth rather than nucleation sites the energy barrier for them to be active should be low enough that the vast majority of them participate solidification. As each particle grows they should each form a single grain in the as-cast structure, resulting in a ratio of one grain formed for each particle remaining. The relationship between number of particles or powders considered and grains formed is shown in Fig. 9b. Once again the same four assumptions are shown, no dissolution or breakup (Introduced Powders), dissolution no breakup (Dissolution), breakup no dissolution (Breakup), and both dissolution and breakup (Dissolution + Breakup). If no breakup is considered more than one grain is formed per powder whether dissolution is considered or not, which does not correspond to an assumption of nucleation or direct particle growth. If only breakup is considered without dissolution then less than one grain is formed per particle, with a ratio between that of AlTiB inoculation of Al and AlTiB inoculation of Ti. However, from the rod dipping experiment we know dissolution occurs so this is also not reflective of the true case. When both breakup and dissolution are considered the ratio of particles to grains formed is close to 1:1 except for the smallest powders. This ratio of one particle to one grain formed is indicative of the absence of a large energy barrier to solidification and supports the theory that the particles are acting as centers of direct epitaxial growth rather than nucleation. The mechanism of isomorphic inoculation by polygranular powders can then be described as a multi-step process. Polygranular powders of the same phase and similar lattice parameter to the matrix are added to the melt. While thermally stable the particles are not diffusively stable in the melt and some dissolution occurs, the grain boundaries preferentially dissolve and the powders break apart into multiple particles which each act as isomorphic inoculants. Upon cooling these particles grow epitaxially, rather than nucleating new solid, and each is responsible for the formation of a grain found in the as-cast structure. Using the molten salt particle heat treatment experiments and particle dissolution in fluid flow model the number of isomorphic inoculants was found to correlate well with the number of grains formed.

5. Conclusions

The mechanism of highly efficient isomorphic inoculation was confirmed to be powder breakup and epitaxial growth. The structure of the particles introduced to the melt was found to be highly plastically deformed with long pancake structured grains that were subdivided into more equiaxed grains as milling progressed, this did not have a large effect on the average grain size within the particles, the main effect of continued cryo milling was the reduction of the powder size. Heat treatment to reproduce the thermal conditions encountered by the powders in the melt resulted in significant grain growth, the extent of which depended more on the size of the powders than their initial microstructure. The dissolution rate of the powders was calculated based on mass transfer of solute through an interlayer, based on the model of Hsu [13] while also taking into account fluid flow, this was validated using a rod dipping experiment. After taking into account dissolution and breakup the number of grains formed during solidification corresponds well with the number of particles formed from the particles which survive the melt indicating that no nucleation barrier needed to be overcome. This confirms the proposed mechanism of highly efficient isomorphic inoculation to be particle breakup and direct particle growth rather than nucleation of new solid.

CRediT authorship contribution statement

J.R. Kennedy: Writing – review & editing, Writing – original draft, Validation, Methodology, Investigation, Formal analysis, Conceptualization. **A.K. Boukellal:** Writing – review & editing, Writing – original

draft, Validation, Investigation, Formal analysis. **E. Brodu:** Writing – review & editing, Writing – original draft, Investigation. **D. Daloz:** Writing – review & editing, Writing – original draft, Investigation. **B. Rouat:** Writing – review & editing, Writing – original draft, Investigation. **E. Bouzy:** Writing – review & editing, Writing – original draft, Supervision, Investigation, Funding acquisition, Formal analysis, Conceptualization. **J. Zollinger:** Writing – review & editing, Writing – original draft, Validation, Supervision, Investigation, Formal analysis, Conceptualization.

Declaration of competing interest

The authors declare that they have no known competing financial interests or personal relationships that could have appeared to influence the work reported in this paper.

Acknowledgments

This work was supported by Région Lorraine and the French State through the program "Investment in the future" operated by the National Research Agency (ANR), France and referenced by ANR-11-LABX-0008-01 (LabEx DAMAS). Additionally work was completed in the framework of the industrial chair in solidification financed by ArcelorMittal Global R&D, ArcelorMittal: Industeel, CEA, and Framatome.

References

[1] M. Rappaz, J.A. Dantzig, Solidification, EPFL Press, 2016.
[2] D.A. Porter, K.E. Easterling, Phase Transformations in Metals and Alloys (2. Auflage ed.), CRC Press, 2004.
[3] A.L. Greer, Grain Refinement of Alloys by Inoculation of Melts, Philos. Trans.: Math., Phys. Eng. Sci. 361 (1804) (2003) 479–495, Publisher: The Royal Society.
[4] B.E. Sundquist, R.A. Oriani, Homogeneous Nucleation in a Miscibility Gap System. A Critical Test of Nucleation Theory, J. Chem. Phys. 36 (10) (1962) 2604–2615.
[5] B.E. Sundquist, On "Nucleation catalysis in supercooled liquid tin", Acta Metall. 11 (6) (1963) 630–632.
[6] F.M. Kuni, A.K. Shchekin, A.I. Rusanov, B. Widom, Role of surface forces in heterogeneous nucleation on wettable nuclei, Adv. Colloid Interface Sci. 65 (1996) 71–124.
[7] Güven Kurtuldu, Philippe Jarry, Michel Rappaz, Influence of Cr on the nucleation of primary Al and formation of twinned dendrites in Al–Zn–Cr alloys: Can icosahedral solid clusters play a role? Acta Mater. 61 (19) (2013) 7098–7108.
[8] T.E. Quested, A.L. Greer, Athermal heterogeneous nucleation of solidification, Acta Mater. 53 (9) (2005) 2683–2692.
[9] J.R. Kennedy, D. Daloz, B. Rouat, E. Bouzy, J. Zollinger, Grain refinement of TiAl alloys by isomorphic self-inoculation, Intermetallics 95 (2018) 89–93.
[10] J.R. Kennedy, A.E. Davis, A. Caballero, A. Garner, J. Donoghue, S. Williams, J. Zollinger, E. Bouzy, E.J. Pickering, P.B. Prangnell, Isomorphic grain inoculation in Ti-6Al-4V during additive manufacturing, Mater. Lett.: X 8 (2020) 100057.
[11] Jacob R. Kennedy, Bernard Rouat, Dominique Daloz, Emmanuel Bouzy, Julien Zollinger, Effect of Inoculant Alloy Selection and Particle Size on Efficiency of Isomorphic Inoculation of Ti-Al, Materials 11 (5) (2018) 666, Number: 5 Publisher: Multidisciplinary Digital Publishing Institute.
[12] T.E Hsieh, R.W. Balluffi, Experimental study of grain boundary melting in aluminum, Acta Metall. 37 (6) (1989) 1637–1644.
[13] Jyh-Ping Hsu, Mon-Jyh Lin, Dissolution of solid particles in liquids, J. Colloid Interface Sci. 141 (1) (1991) 60–66.
[14] M Boivineau, Claus Cagran, D Doytier, V Eyraud, M-H Nadal, Boris Wilthan, Gernot Pottlacher, Thermophysical properties of solid and liquid Ti-6Al-4V (TA6V) alloy, Int. J. Thermophys. 27 (2) (2006) 507–529.
[15] R.r. Keller, R.h. Geiss, Transmission EBSD from 10 nm domains in a scanning electron microscope, J. Microsc. 245 (3) (2012) 245–251, _eprint: https://onlinelibrary.wiley.com/doi/pdf/10.1111/j.1365-2818.2011.03566.x.
[16] Glenn C. Sneddon, Patrick W. Trimby, Julie M. Cairney, Transmission Kikuchi diffraction in a scanning electron microscope: A review, Mater. Sci. Eng. R 110 (2016) 1–12.
[17] Etienne Brodu, Emmanuel Bouzy, Jean-Jacques Fundenberger, Julien Guyon, Antoine Guitton, Yudong Zhang, On-axis TKD for orientation mapping of nanocrystalline materials in SEM, Mater. Charact. 130 (2017) 92–96.
[18] B. Beausir, J.J. Fundenberger, Analysis tools for electron and X-ray diffraction, ATEX-Softw. 201 (7) (2017) www.atex-software.eu, Université de Lorraine-Metz.
[19] Irene J. Beyerlein, László S. Tóth, Texture evolution in equal-channel angular extrusion, Prog. Mater. Sci. 54 (4) (2009) 427–510.
[20] D. Kuhlmann-Wilsdorf, Niels Hansen, Geometrically necessary, incidental and subgrain boundaries, Scr. Metall. Mater. 25 (7) (1991) 1557–1562.
[21] László S. Tóth, Yuri Estrin, Rimma Lapovok, Chengfan Gu, A model of grain fragmentation based on lattice curvature, Acta Mater. 58 (5) (2010) 1782–1794.
[22] D.A. Hughes, N. Hansen, High angle boundaries formed by grain subdivision mechanisms, Acta Mater. 45 (9) (1997) 3871–3886.
[23] T.R. Malow, C.C. Koch, Grain growth in nanocrystalline iron prepared by mechanical attrition, Acta Mater. 45 (5) (1997) 2177–2186.
[24] Tao Wang, Hongzhen Guo, Lijun Tan, Zekun Yao, Yan Zhao, Penghui Liu, Beta grain growth behaviour of TG6 and Ti17 titanium alloys, Mater. Sci. Eng. A 528 (21) (2011) 6375–6380.
[25] V.T. Witusiewicz, A.A. Bondar, U. Hecht, T.Ya. Velikanova, The Al–B–Nb–Ti system, J. Alloys Compd. 472 (1–2) (2009) 133–161.
[26] T.K. Sherwood, R.L. Pigford, C.R. Wilke, Mass Transfer, McGraw-Hill, 1975.
[27] H. Schlichting, K. Gersten, Boundary-Layer Theory, Springer, 2016.
[28] C.T. Crowe, Multiphase Flows with Droplets and Particles, CRC Press, 2012.
[29] I. Egry, D. Holland-Moritz, R. Novakovic, E. Ricci, R. Wunderlich, N. Sobczak, Thermophysical Properties of Liquid AlTi-Based Alloys, Int. J. Thermophys. 31 (4–5) (2010) 949–965.
[30] Peter T.B. Shaffer, Plenum Press Handbooks of High-Temperature Materials, Springer US, Boston, MA, 1963.
[31] K. Zhou, H.P. Wang, J. Chang, B. Wei, Surface tension measurement of metastable liquid Ti–Al–Nb alloys, Appl. Phys. A 105 (1) (2011) 211–214.